Monitoring changes in pulse profile shape in the X-ray binary Her X-1

Hongyu Zhang,[1] McKinley Brumback ⬤,[2] and Fiona Harrison[2]

[1]*Department of Physics, Hamilton College, 198 College Hill Road, Clinton, NY, 13323, USA*
[2]*Cahill Center for Astronomy and Astrophysics, California Institute of Technology, 1216 E California Blvd, Pasadena, CA 91125, USA*

ABSTRACT

Accreting neutron star binaries provide test grounds for high energy physics under extreme gravitational and magnetic fields. In this study, we chose our source to be a low-mass X-ray binary Her X-1 with a 35-day superorbital modulation, a periodic change in X-ray flux with a periodicity longer than orbital period. While we have a simplistic, warped precession model of the accretion disk to account for the superorbital period, we have yet determined whether changes in soft pulse profile to be smooth, indicating a pure disk rotation, or stochastic, implying short term changes in emission or irregularities in disk. NICER's high-cadence data makes it possible to see detailed changes in soft pulse profile, and precisely constrain the geometry of the accretion disk. Our data set consists of 15 consecutive observations in a single superorbital cycle, out of which four occur during the bright "main-on" stage with strong pulsations and detailed pulse profiles. In an energy resolved pulse profile study, we found clear pulsation signals in both soft and hard energy bands. In both soft and hard pulse profiles, we observed fine features which change over time. Our simplistic precessing accretion disk model was not able to reproduce these features, and this may suggest more complex accretion structure. With limited high energy signal, we best fitted the spectra of these data by an absorbed power law, a black body component and two/three gaussian emission lines. We saw consistent spectral constraint during the main-on phase.

1. INTRODUCTION

The Harrison group researches in observational and experimental high energy astrophysics, with the X-ray astronomy being its primary interest (Harrison et al. 2013). One of the main sources of cosmic X-ray is the accretion process where a stellar companion transfers its gas onto a magnetically dominated neutron star. Studying how matter behaves under extreme gravitational and magnetic fields gives deep insights into physics at high energy. We have had a general picture of the accretion process. The accretion disk is formed by the mass transfer from the companion to the neutron star due to Roche lobe overflow. A structure known as an accretion stream is formed when the gas is funneled along the magnetic field lines of the neutron star onto the magnetic poles (Romanova et al. 2004). However, we have yet to observationally constrain these complex accretion structures.

Among the luminous X-ray binaries, LMC X-4, SMC X-1 and Her X-1 are well known and studied for their superorbital periods, variations of luminosity on a period longer than orbital periods, on the scale of 30 - 60 days. Brumback et al. (Brumback et al. 2020, 2021) have successfully used a precessing, warped accretion disk model proposed by Hickox and Vrtilek (Hickox & Vrtilek 2005) to account for the superorbital feature of these X-ray sources. When the hard pulsar beam directs towards inner region of the accretion disk, the light is reprocessed through blackbody radiation in soft X-ray, which allows study of detailed accretion disk geometry.

For Her X-1 in particular, it is a bright, well-known cyclotron source. It is a low mass X-binary with a 1.5 $M_\odot$ neutron star and 2.2 $M_\odot$ A/F type star (Brumback et al. 2021). The rotation of the binary give Her X-1 a 1.7-day orbital period. Pre-eclipse dips are seen for every 1.62 days. (Jones & Forman 1976) They are thought to be caused by the material coming out of the inner Lagrangian point blocking the X-ray. (Shakura et al. 1999) Her X-1 is one of a few persistent neutron star binaries whose accretion disk is viewed edge-on (i $\sim$ 85 degree) as seen from Earth. This effect allows us to simultaneously probe its pulsar beam and the accretion disk

geometry. Her X-1 is a cyclotron line source, (Truemper et al. 1978) which has a board absorption feature that allows astronomers to directly measure the its magnetic field strength.

Similarly to Brumback et al.(2021), we assume the 35-day superorbital modulation of Her X-1 is caused by the precession of the warped accretion disk. The superorbital period is characterized into a bright, 11-day "main-on" phase when observer has an direct view on the pulsar, and a fainter, 8-day "short-on" phase there is obscuration of the pulsar by the accretion disk. We chose our observation window to be during the main-on phase to have the highest timing resolution.

While observational data have been taken on the magnetic accretion stream by NuSTAR and XMM-Newton, the changes in the soft pulse profile have not yet been determined whether to be smooth, indicating a pure disk rotation, or stochastic, implying disk or emission structure having short term changes (Brumback et al. 2021). In addition, this prototype source has never been observed with NICER(Neutron star Interior Composition Explorer), which offer high-cadence data, and particularly bandpass coverage at low energy range (< 3 keV) lacked from observatories like NuSTAR. It is now possible to get insight into the changes in the soft pulse profile, and constrain the geometry of the accretion disk to an unprecedented precision. Furthermore, a complete data set can serve as a testbed for more intricate hydrodynamical theory on accretion physics (Romanova et al. 2004).

For this study, we expect to follow the method of Brumback et al.(2021) (referred as B21 thereafter) to perform phase-averaged and phase-resolved spectroscopy. Importantly, we will obtain pulse profile using all fifteen short-term observations from NICER during a single main-on state of Her X-1. This allows us to examine changes in accretion steam in short periods and geometry of the accretion disk in detail.

In section 2 we show where our aimed observations and actual observations are in a superorbital period. We describe the method for performing spectroscopy and extracting pulse profiles in section 3 and interpret the results in section 4. In section 5, we describe our attempt of modeling with warped accretion disk.

2. OBSERVATIONS

To obtain pulse profiles with detailed features, one very important criteria is a high X-ray flux, which produce a high signal to noise ratio. In order to achieve it, it is necessary to make sure the observations do not occur during an eclipse or pre-eclipse dip, in addition

Table 1. Description of Her X-1 Observations

Date (YMD)	Observation ID
2020-10-24	3602010101
2020-10-24	3602010102
2020-10-25	3602010103
2020-10-25	3602010104
2020-10-26	3602010105
2020-10-26	3602010106
2020-10-27	3602010107
2020-10-27	3602010108
2020-10-28	3602010109
2020-10-28	3602010110
2020-10-29	3602010111
2020-10-29	3602010112
2020-10-30	3602010113
2020-10-31	3602010114
2020-10-31	3602010115

to that they are planned to occur during an main-on superorbital phase.

Our data consist of fifteen consecutive observations taken by NICER of Her X-1 from 24 October 2020 to 31 October 2020. These observations, due to the fact that these are a single set of observation from a single telescope on a single target, will be referred as observation 01, 02 ⋯ 15. Table 1 shows the date of observations and observation ID numbers. Figure 1 shows the Swift/BAT light curve in black showing three 35-day superorbital periods. We plotted the blue and red vertical lines to indicate starting times of all fifteen observations. Clearly, not all fifteen observations fall on to the main-on phase as planned. Instead, from looking at the superorbital light curve plotting alone, roughly the first half of observations appear to be during the main-on phase. Calculation of the timing of orbital eclipses shows that observation 02, 12, 13 and 15 are during an eclipse.

We used HEASoft version 6.28 for data reduction. The version of NICERDAS is 2020-04-23_V0007a. We used the nicerl2 pipeline with the "3C50" background model (Remillard et al. 2021). We also filtered the data using the planetary K-index(kp-index) with kp-index < 5. This this into the account of the fluctuation disturbance of the local magnetic fields usually caused by solar winds.
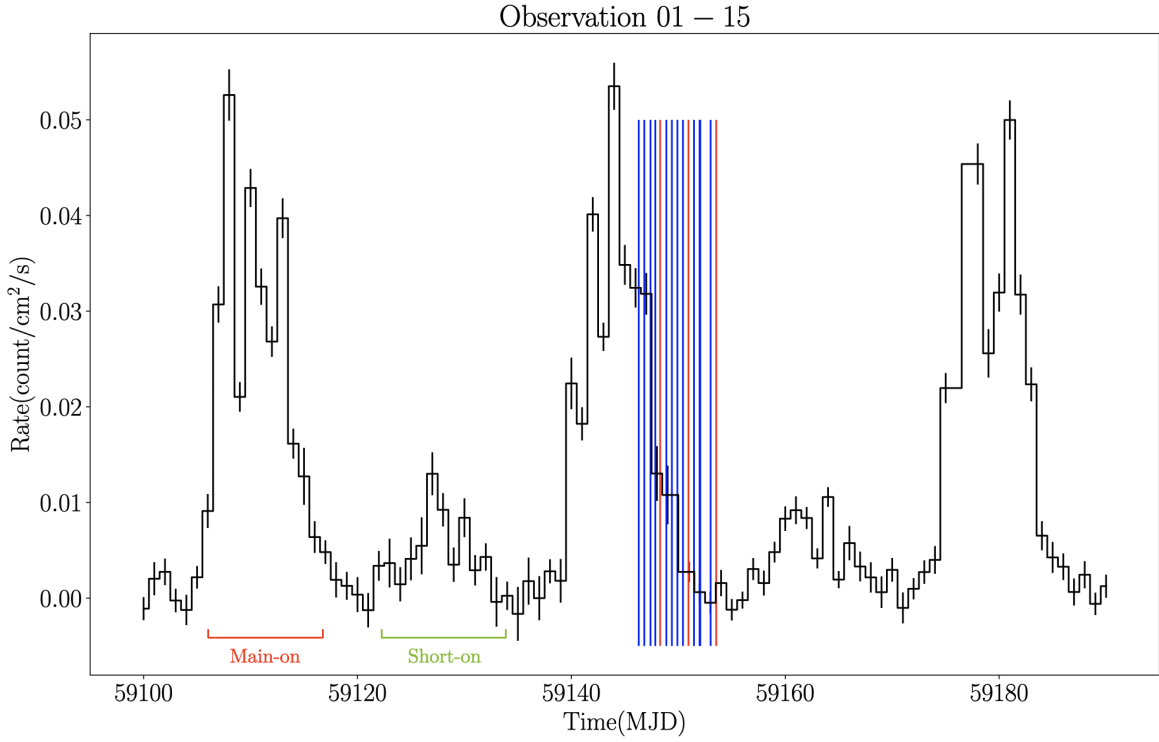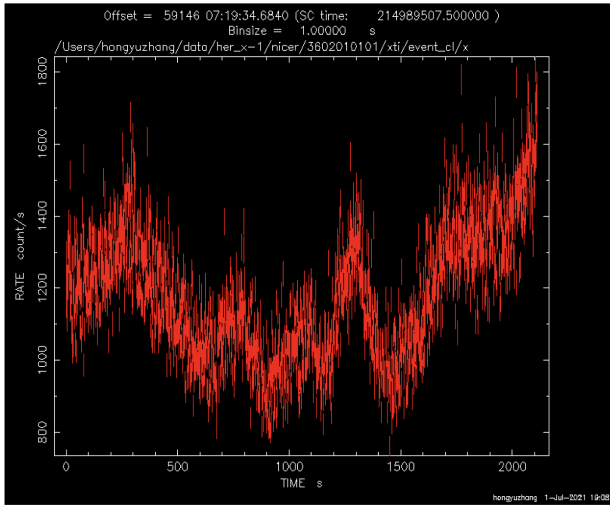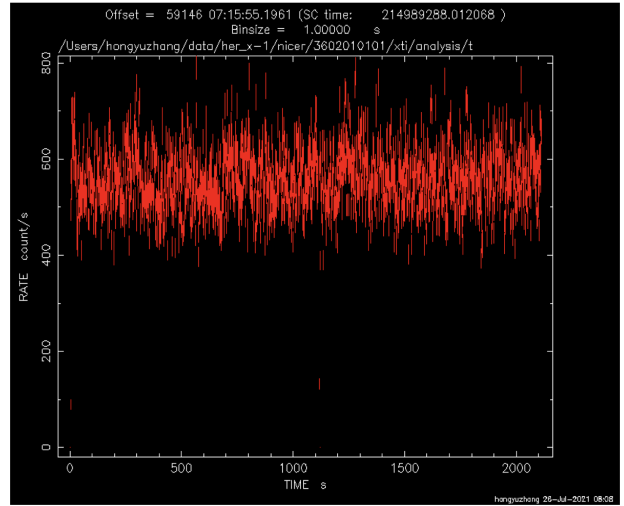
Observation 01 − 15

Figure 1. Shown in black mid-step function, is the light curve of Her X-1 using the BAT(Swift's Burst Alert Telescope) data, which shows three 35-day superorbital periods. Vertical lines show instances where starting times of the observations fall on the superorbital period. The red lines indicate observation 05, 10 and 15, from left to right. The thick blue line is the overlapped observation 12 and 13. The main on phase is marked with red bracket while short-on in blue. It is clear that majority of the observation fell out of the range of the main on phase.

Unfiltered light curve of observation 01   Filtered light curve of observation 01

Figure 2. Comparison between filtered and unfiltered light curve of observation 01 with binsize = 1s.

Figure 2 shows the unfiltered and the filtered light curves of the first observation. This is our brightest observation with the highest photon count rate. Filtering, in this context, mainly indicates leaving out the photons that are not in the calibrated range of NICER: $0.3 - 12$ keV, giving a "flat" profile to the filtered light curve. This is in addition to the background filtering mentioned.

To further determine which observations are suitable for our analysis, we extracted and filtered light curves for observation 01 through 12. We also attempted extracting pulse profiles from all 12 observations to determine if we could see detailed features. We disregarded observation 13 through 15, because observation 12 already has count rate on the magnitude of 5 counts/second, the latter observations in a lower superorbital states with two in an eclipse are not expected to have high enough of a count rate. Expected from the transition into a lower superorbital state, count rate of the filtered light curves shows a general trend of decreasing: ranging from ~ 600 counts/second of observation 01 to ~ 20 counts/second of observation 11. Also expectedly, observations in eclipses showed dramatically lower count rate than ones next to them. In addition, we suspect that observation 05 happened during an pre-eclipse dip. Its filtered light curve showed large fluctuations in count rate, which results inconsistency in pulsation strength, and therefore is disregarded. We then categorized the rest of the observations into three groups: first, observation 01, 03, 04 and 06 that showed high count rates (≥ 350 counts/second) and strong pulsation signals; second, observation 07 - 09 in the transition period from the main-on to the low state with lower count rate (~ 60 counts/second) and irregular pulsation occurrence.[1]; third, observation 10 - 12 with extremely low count rate (~ 20 counts/second)w and no pulsation at all. Therefore, we shifted our focus on the first four "good" observations: 01, 03, 04 and 06.

3. DATA ANLYSIS

We follow Brumback et al. (2021) to do data analysis in two parts, spectral and timing. We firstly perform phase-averaged spectroscopy, which analyzes the energy of the detected photons regardless of the timing of detection; then we preform the timing analysis, in which we search for the spin period of the pulsar and fold the light curve by the spin period to obtain pulse profiles.

3.1. *Phase-averaged spectroscopy*

---

[1] Irregular means pulsation can be searched in certain observations without a clear reason

We use the filtered light curves described in section 2 and group them with 100 counts per bin. In the fitting process, we noticed anomalies in the data below 0.5 keV and above 10 keV. Therefore, we further energy filtered light curves to the range of 0.5 keV-10 keV. In fact, the reduced chi-sqaured value before the energy filtering could only go as low as 5.

We performed spectral analysis on the first ten observations with Xsepc version 12.11.1. The first four "good" observations, or the first category of the observation, show consistent and physical constraint on parameters. In the second category of observations 07 - 09, only 08 shows physical parameters but noticeably starts to lose constraint. Observation 10 shows physical parameters values, but completely loses the constraint over parameters. The decrease in spectral constraint is consistent with the increase in obscuration of the pulsar by the accretion disk. This is also the reason we did not perform spectral fit beyond observation 10.

Similar to B21, we used an absorption powerlaw and soft blackbody component for the X-ray spectra. In addition, we added a gaussian emission line for the ~ 0.9 keV feature and another one at 6.4 keV for iron line for our first spectral model. The "bump" at 0.9 keV has been recorded for Her X-1 with XMM-Newton's RGS instrument (Jimenez-Garate et al. 2002) and pointed out in B21 to be composed of complex emissions from Ne, Fe and more. NICER does not have the resolution to resolve this feature. We therefore follow B21 to continue using a broad Gaussian line to capture it. For our second model, We additionally added a broader ($\sigma \leq 0.4$) emission line feature at 6.4 keV for better fit. This is the model used in B21. Different from B21, we cannot constraint the cutoff energy of the powerlaw. This is reasonable since the B21 result of cutoff energy is around 19 keV, which is beyond the range of NICER's calibrated range.

For the preliminary result, we used the averaged result from HEASARC N_{H} calculator with the HI4PI Map for the absorbing column density, which is $1.54 \times 10^{20} \, \mathrm{m}^{-2}$. We used the multiplicative parameter `TBabs`. In order for the parameter to not be degenerate, we fixed it across all spectral fits. Note that although Her X-1 is a cyclotron source, we did not fit the cyclotron resonance scattering feature for it is at 36 keV and way above the range of NICER (Brumback et al. 2021).

Figure 3 shows the phase averaged spectra for the four good observation and two best fit models for each observation with two and three gaussian line component each. For each subfigure, we present the data with additive model compnant in the top panel, ratio plot of data to model in the middle panel, and the chi squared

plot in the bottom panel. We notice that the iron line model component could never be constrained by statistical fit, neither could the sigma value for the broader Gaussian line at about 6.4 keV. Therefore, we had to fix the energy for the iron line, and sigma for both narrow and broad line at 6.4 keV. We present all the parameters in table 2.

We do not present the spectral result beyond the first category of observation for the lack of parameter consistency beyond observation 06.

3.2. *Timing Analysis*

To determine the spin frequency and the time derivative for each observation, we used HENDRICS's `folding_search`. Consistent with the B21 result, we found that the derivative of spin period is on the magnitude of 10^{-8} and therefore negligibly small. We calculated the uncertainty in the spin period by matching the phase difference between the pulse profile at the beginning and the end of each observation. We did not calculate the spin period and its derivative for observation 02 since we could not detect pulsation; neither did we calculate for observation 05 due to the weak pulsation signal. We were, surprisingly, able to detect pulsation and extract pulse profiles for observation 07 and 09, from which we could not constrain spectral parameters. Their pulsations were expected weak and they lost all the detailed features that we could see from the first four good observations. Therefore, we did not calculate the frequency and frequency derivative for them. In addition, we could not detect pulsation beyond observation 09. The result is presented in table 3.

We can now perform extraction of pulse profiles in order to observe changes in their features. Firstly we performed an energy-resolved timing analysis to have a fine image of the transition between soft and hard pulse profile. We particularly want to see where soft pulse profile start to change to harder shape. Since the NICER's photon count decreases as energy increase, we increase the energy intervals appropriately: from $0.5 - 1.5$ keV, the interval is 0.1 keV per range; from $1.5 - 4.5$ keV, it is 0.5 keV per range; then we used $4.5 - 6.5$ keV and $6.5 - 10.0$ for harder X-ray. However, by studying the energy ranging of the 0.9 keV Gaussian emission line seen in figure 4, we do have expectation from spectroscopy that soft X-ray emission will be most eminent from the $0.5 - 0.6$ keV range and hard X-ray pulse profile will be similarly shaped above 1.5 keV. We

still need to rely on the energy resolved pulse profile to see how the 0.9 keV line behave.

Using the result from the energy-resolved pulse profile, we filtered three main energy ranges: 0.5 - 0.6 keV where there is most soft, reprocessed features; 0.5 - 1.4 keV or 0.5 - 1.4 keV for the 0.9 keV emission line; and 1.4/1.5 - 10 keV for the hard pulse profiles. The result from energy-resolved pulse profile indicates the hard energy range of 1.4 - 10 keV cannot be applied to observation 06 since the shape of the pulse profiles varied more much compare to the other three observations. To further verify this result, we calculated Pulse Fraction $(PF) = (P_{max} - P_{min})/(P_{max} + P_{min})$, where P_{max} is the maximum pulsation and P_{min} is the minimum, for each energy intervals of the energy-resolved spectroscopy. The uncertainty just come from simple uncertainty rules where the uncertainty of sum is sum of uncertainties and uncertainty of a product is the sum of fractional uncertainties. The pulse fraction plots for observation 01, 03 and 04 are shown in figure 5.

Then we could use the Stingray's `fold_events` to create pulse profiles using the three main filtered energy ranges. The results are shown in figure 6. We used 128 bins/phase for observation 01, 03 and 04 because of their high timing resolution, and 64 bins/phase for observation 06 for the decreased resolution.

4. RESULTS

4.1. *Phase-averaged spectroscopy*

We find from our analysis that a single absorbed powerlaw, a soft balckbody component suffice to provide a good description for the X-ray spectrum of Her X-1, because all of our parameters (photon index, kT, LineEs for all three gaussian lines) are in line with spectral analysis of B21's observation H1 and H4. Their values are also all close to each other. The general trend of decrease in normalization values can be explained by the decrease in X-ray flux during the end of the superorbital period.

Although not included in the table, it is worth mentioning again that component parameters for observation 08 and 10 are on the same order of magnitude as our four good observation but they decreased overall with time. This is again a result of obscuration of the pulsar.

4.2. *Pulse Profiles*

Her X-1's energy-resolved pulse profiles and pulse fraction plots (Figure 6, Figure 5) all show that Observation 01, 03 and 04 are similarly shaped in both soft and hard energy bands. The hard pulse profile for observation 06 has its shape completely changed and it is much weaker
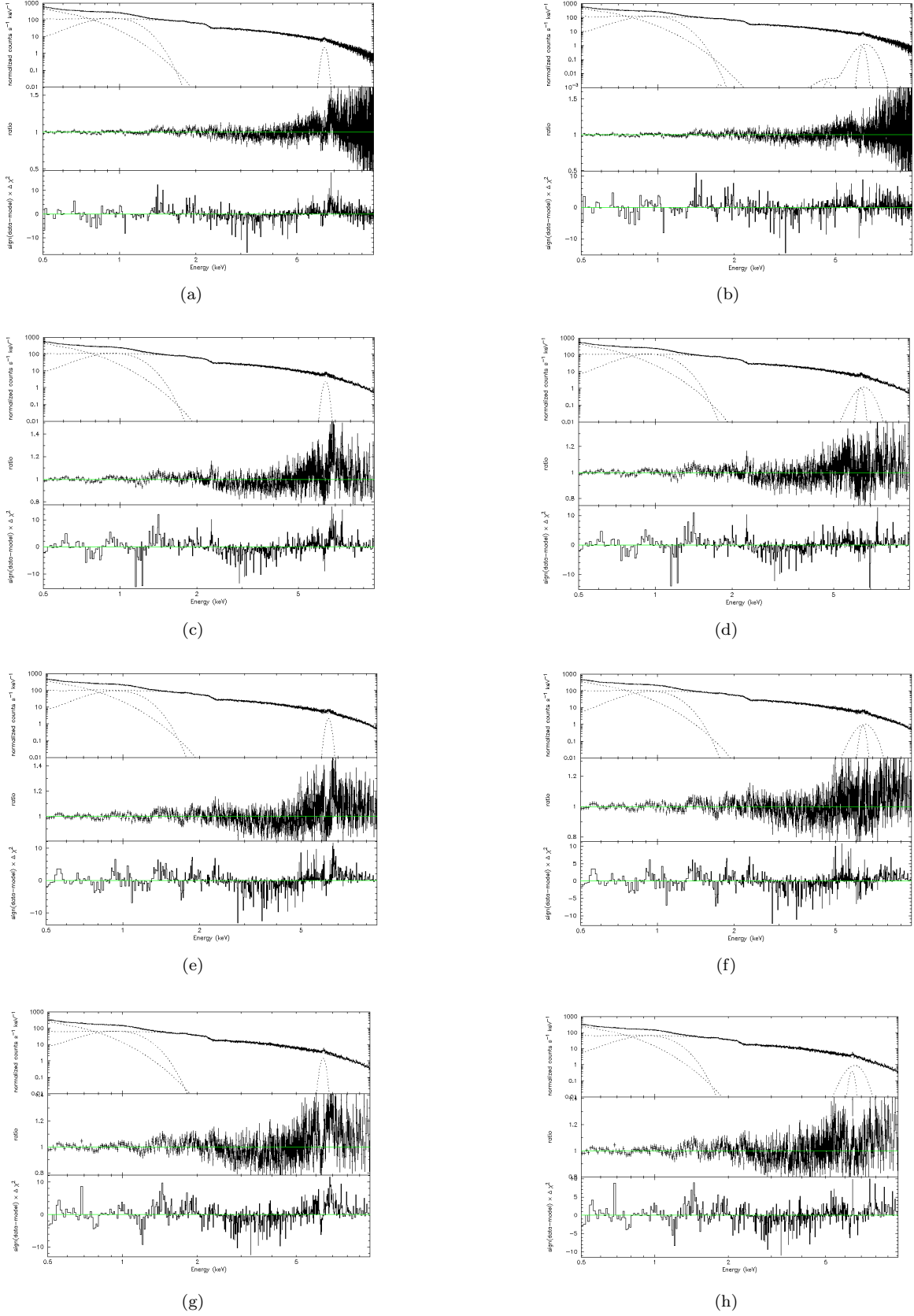
Figure 3. NICER spectra for the Her X-1 observation (a) observation 01 (2 gaus), (b) observation 01 (3 gaus), (c) observation 03 (2 gaus),(d) observation 03 (4 gaus), (e) observation 04 (2 gaus), (f) observation 04 (3 gaus), (g) observation 06 (2 gaus) and (h) observation 06 (3 gaus). For each spectrum, the top panel shows the spectrum and the additive components of the best fit model, the middle panel is the plot of the ratio of the data to model, and the bottom panel shows the chi squared plot.

Table 2. Her X-1 phase averaged spectroscopy parameters

Model	Component	Parameter(unit)	Observation 01	Observation 03	Observation 04	Observation 06
	TBabs	nH(10^{22})	0.0154	0.0154	0.0154	0.0154
	Powerlaw(fixed)	PhotoIndex	0.812	0.833	0.829	0.805
	powerlaw	norm	7.57×10^{-2}	7.07×10^{-2}	6.53×10^{-2}	4.19×10^{-2}
	bbody	kT(keV)	0.101	0.101	0.103	0.101
	bbody	norm	3.89×10^{-3}	3.72×10^{-3}	3.01×10^{-3}	2.19×10^{-3}
2gaus Model[a]	gaussian	LineE(keV)	0.916	0.918	0.919	0.904
	gaussian	Sigma(keV)	0.189	0.195	0.193	0.211
	gaussian	norm	4.25×10^{-2}	3.86×10^{-2}	3.23×10^{-2}	2.49×10^{-2}
	gaussian(fixed)	LineE(keV)	6.40	6.40	6.40	6.40
	gaussian(fixed)	Sigma(keV)	0.100	0.100	0.100	0.100
	gaussian	norm	2.08×10^{-3}	2.26×10^{-3}	1.97×10^{-3}	1.33×10^{-3}
	TBabs	nH(10^{22})	0.0154	0.0154	0.0154	0.0154
	Powerlaw(fixed)	PhotoIndex	0.835	0.858	0.851	0.837
	powerlaw	norm	7.70×10^{-2}	7.21×10^{-2}	6.65×10^{-2}	4.30×10^{-2}
	bbody	kT(keV)	0.102	0.101	0.104	0.102
	bbody	norm	3.84×10^{-3}	3.66×10^{-3}	2.97×10^{-3}	2.14×10^{-3}
	gaussian	LineE(keV)	0.919	0.923	0.923	0.914
3guas Model[b]	gaussian	Sigma(keV)	0.185	0.190	0.187	0.201
	gaussian	norm	4.06×10^{-2}	3.65×10^{-2}	3.07×10^{-2}	2.29×10^{-2}
	gaussian$_{narrow}$(fixed)	LineE(keV)	6.40	6.40	6.40	6.40
	gaussian$_{narrow}$(fixed)	Sigma(keV)	0.100	0.100	0.100	0.100
	gaussian$_{narrow}$	norm	7.74×10^{-4}	1.03×10^{-3}	8.09×10^{-4}	3.63×10^{-4}
	gaussian$_{broad}$	LineE(keV)	6.62	6.64	6.56	6.62
	gaussian$_{broad}$(fixed)	Sigma(keV)	0.400	0.400	0.400	0.400
	gaussian$_{broad}$	norm	7.74×10^{-3}	4.08×10^{-3}	3.46×10^{-3}	3.17×10^{-3}

[a] For the 2gaus model, the component is `TBabs*(pow+bbody+gaus+gaus)`
[b] For the 3gaus model, the component is `TBabs*(pow+bbody+gaus+gaus+gaus)`

Table 3. Best fit spin frequency for Her X-1 Observations

Observation	Spin Frequency(s^{-1})
01	0.807951(5)
03	0.807935(6)
04	0.807930(5)
06	0.80792(1)
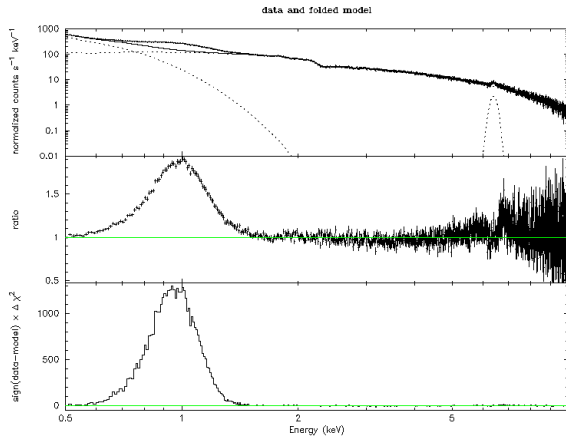
Figure 4. The 0.9 keV "bump" showing its shape in ratio plot and chi squared plot after fitting and removing the 0.9 keV gaussian line component

than the other three observations. This suggests that this observation occurs near the starting point of the accretion disk obscuration. In agreement with B21's observation H1 and H4, the main soft peak is near 180° out of phase with the main hard peak. Due to the shorter than expected duration of the observation window, we could not conclude if there is a relative phase shift between the soft and hard peaks, which was identified in B21.

In observation 01, 03 and 04, all of the hard pulse profiles (purple) captured the narrow main peak as B21 did. However, we did not identify the notch in the main hard peak. Notably in observation 01 and 03, we captured smaller, tertiary peaks that reside in the broader secondary peak described by B21's observation H4. It may be the random fluctuation as mentioned in Brumback et al. (2021). But the fact that these tertiary peaks are consistent in observation 01 and 03 but fade in observation 04 and disappear in observation 06 may be explained by the obscuration of the pulsar by the accretion disk occurs around the time of the observation. For observation 01, 03 and 04, the two tertiary peaks appeared simultaneously as the energy increases. How-

ever, for observation 06, the tertiary peak on the left appeared at lower energy (0.5 - 1.0keV) and right peak appeared at higher energy (1.0 - 1.5 keV).

The initial purpose of the study is to observe detailed changes in soft pulse profile in its main-on phase with fifteen spanning observations. The apparent shapes of the pulse profile stay similar for all four observation and almost the same for the first three observation. But with only four good data sets occurring at the very end of the main-on phase, we cannot come to an conclusive result if the soft pulse profile changes throughout the main-on phase; neither can we identify the change of the soft peak in the observation 06 is due to during-main-on precession or post-main-on obscuration.

5. WARPED ACCRETION DISK MODELING

We followed B21 to further constrain the geometry of the precessing inner accretion disk with the Hickox & Vrtilek (2005) model. The description of the model can be found in the original paper Hickox & Vrtilek (2005). In the model, we assume that the soft X-ray emission is composed of a blackbody emission below 1keV and the hard X-ray emission can be described by a powerlaw.

Our simplistic model is consisted of a series of concentric circles that are tilted and twisted with respect to one another. Its paramters include inner and outer radius (r_{in}, r_{out}) of the rings, their inner and out tilt angle $(\theta_{in}, \theta_{out})$ and the phase offset between the two disks (θ_{off}). We also have the observer angle (θ_{obs}). The pulsar component of the model consists of two type of pulsar beams: a narrow "pencil beams" and wider "fan beams". With limited time at the end of the SURF program, we explored large dimensions in the parameter space of the pencil beam only. It is defined by the angle out of the rotational plane (θ_b), the longitudinal location, or the azimuthal angle of the beam location (ϕ_b) and beam's two dimensional Gaussian width width (σ_b)

The model simulate the pulse profile with the same physical process where the hard pulse profile is generated by calculating the luminosity from the pulsar beam as a function of phase and precession angle, and the soft pulse beam is calculated to represent the reprocessed radiation from the accretion disk.

In our exploration, we are not just interested in the physical parameter values that can be referred to B21, we are also interested in how the model behaves under the most extreme cases like a 90° tilt angle for the outer disk. We present our most interesting result here.

We found that for most of the parameters, large variations change the shape of the pulse profile in a significantly noticeable way that is different from the our physically generated pulse profiles. These parameters are
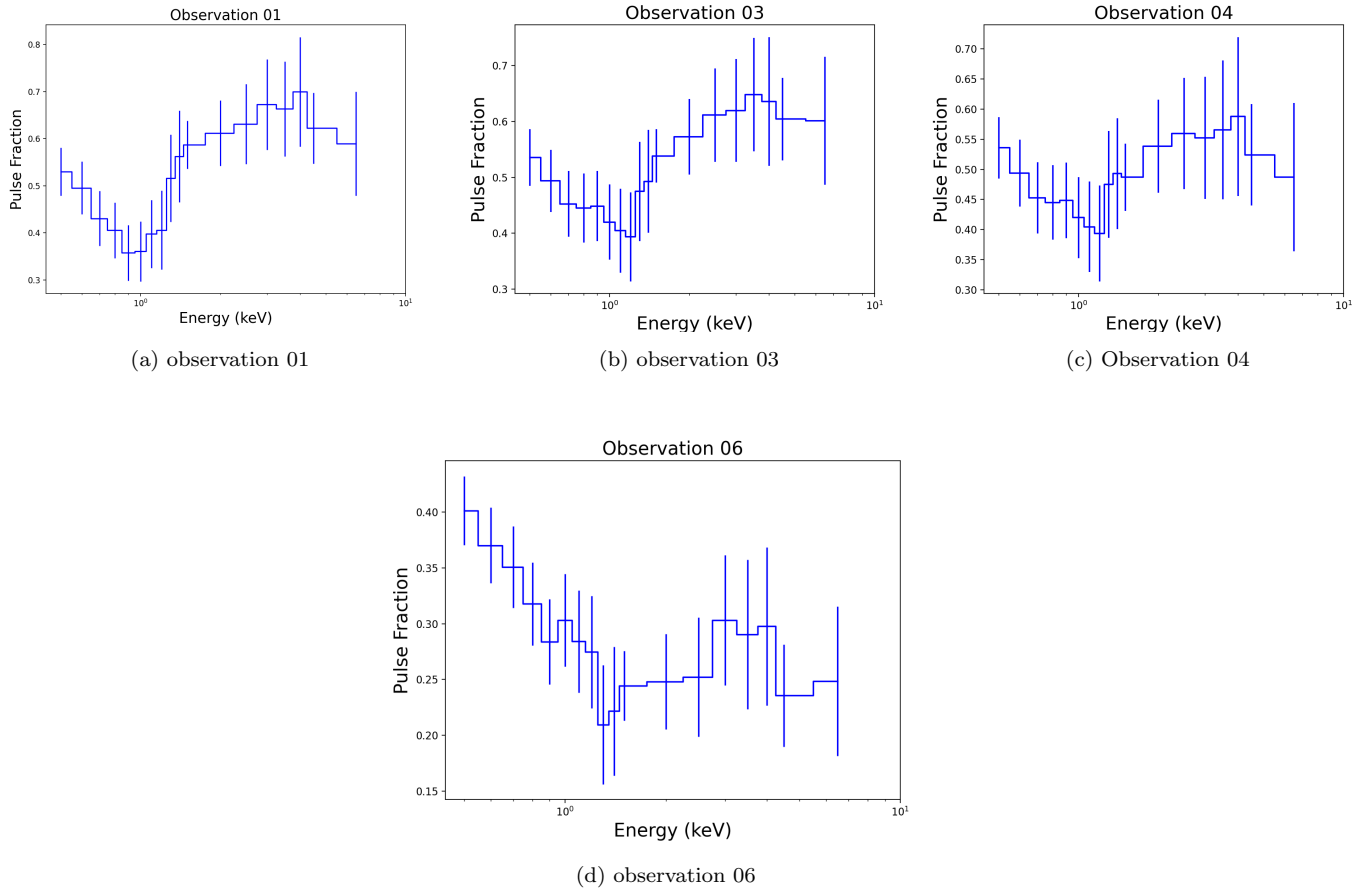
(a) observation 01

(b) observation 03

(c) Observation 04

(d) observation 06

Figure 5. Pulse fraction plots for (a) observation 01, (b) observation 03, (c) Observation 04 and (d) Observation 06. While all of observation 01, 03 and 04 are similarly shaped and had stronger hard pulsation in the hard X-ray range, observation 06 had stronger soft than hard X-ray pulse profile, a strong indication of obscuration of the pulsar by the accretion disk.

θ_{obs}, θ_{b}, ϕ_{b} and θ_{off}. In other words, we conclude that these parameters are better constrained. On the other hand, changing the tilt angles of the inner and outer rings finely tunes the soft pulse profile shape whereas changing the beam widths finely tunes the width of the main and secondary hard peak, which is physically reasonable.

In our attempts, we tried to reproduce the main features that differentiate our new data from the B21 data. These feature includes the noticeable "flat" top of the soft pulse profile, the phase alignment between the main soft peak and the secondary hard peak most noticeable in figure 6 (b), and the fact that the main hard peak is much narrower than the secondary hard peak.

Table 4 present the parameters for our most interesting result by far. And we present here four most interesting pulse profiles and their corresponding disk and beam geometries in figure 7 and 8, respectively. Notice that we changed the outer tilt angle to be the most extreme case of 90°, which is far off from the 30° reported in B21 and previous literature. However, it seems to

be the only way to produce the flat soft peak (7 (c)), which was not seen before. It is physically reasonable, because the if the surface of the accretion disk is orthogonal to the pulsar beam, the illuminated region changes insignificantly with a minor change in spin phase. It was also interestingly able to reproduce the rounded top of the soft pulse profile found in B21 at phase 0.650, seen in figure 7 (d).

We were also able to have the double peaked pattern (figure 7 (a,b)) in the soft pulse profile similar to the pulse profiles from our physical data in the energy range between the fully soft and hard energies (colored in blue in figure 6). It was interesting to see how the secondary soft peaks change height throughout the superorbital phase, as seen in figure 7 (a) and (b). Notice that around phase 0.3, the soft and hard pulse profiles are much better aliened than other phases. We also see much more variations of how the two secondary soft peaks are positioned in other phases. Although our physical data shows that these peaks are actually features from the
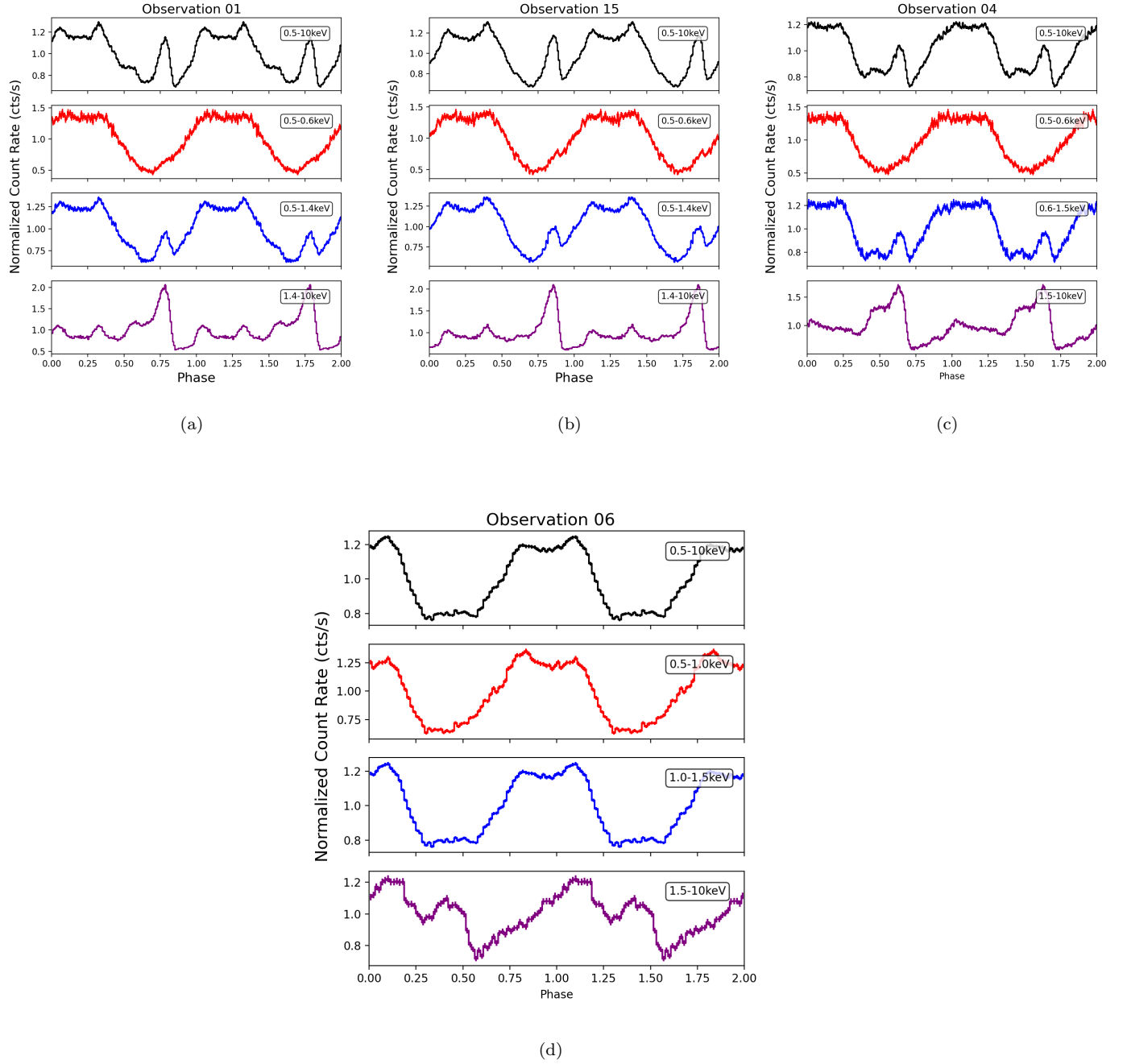
(a)   (b)   (c)

(d)

Figure 6. Pulse profiles for (a) observation 01, (b) observation 03, (c) Observation 04 and (d) Observation 06. Observation 01 and 03 are similarly shaped soft and hard pulse profiles. Observation 04 starts to show changes in hard pulse profile while still having similarly shaped soft pulse profile. Observation 06 had its hard pulse profile's shape completely changed and it is much weaker than previous observations. Note that there are two tertiary peaks in hard pulse profile for observation 01, 03 and 06, and they appear to be at the same phase as the edge of the soft main peak. These peaks strengthen simultaneously as the energy increase. However, for observation 06, there is a energy difference where the left peak appeared at lower energy (0.5 - 1.0 keV) and right peak appeared at higher energy (1.0 - 1.5 keV). The data overall shows strongly the obscuration of the pulsar by the accretion disk.

Table 4. Disk Model Parameters

Component	Parameter
r_{in} (10^8 cm)	0.8
r_{out} (10^8 cm)	1
Inner tilt θ_{in} (°)	0
Outer tilt θ_{out} (°)	90
Phase offset angle θ_{off} (°)	130
Beam 1 Angle from rotation plane θ_{b1} (°)	0
Beam 2 Angle from rotation plane θ_{b2} (°)	60
Beam 1 azimuth ϕ_{b1} (°)	0
Beam 2 azimuth ϕ_{b2} (°)	210
Beam 1 Gaussian half-width σ_{b1} (°)	22.5
Beam 2 Gaussian half-width σ_{b2} (°)	60
Observer elevation θ_{obs}	-5

hard pulse profile, it is nevertheless interesting to have a simplistic model reproducing a fine feature like this.

Due to the limited time, we did not fit the simulated pulse profile to the observed pulse profile. Since the program has ended, the further exploration of the disk model and other physical constraints are deferred to a later time.

6. DISCUSSION

We assume, according to previous studies, that change in pulse profile shape of Her X-1 is caused by reprocessing in the inner accretion disk while it is recessing. In this project, we used fifteen observations in a single superorbital cycle to observe detailed changes in the pulse profiles.

Since we have about half of our observation taken after the main-on superorbital phase, we expect the ones at the end of the main-on phase to have similar shapes but small changes from one observation to another. We can confirm this expectation from the changes we see in our four good observations, which had similarly shaped soft pulse profiles and slightly changed hard pulse profiles. We also expect to see good spectral constraint for the observations during the main-on superorbital phase while losing constraint after obscuration of the pulsar. We can also confirm this expectation from our result of spectral analysis.

In our fifteen observations, we experienced multiple eclipses and one pre-eclipse dip. While those phenomena are interesting for their own sake, they exceed the purpose of our study. In our exploration of the warped accretion disk model with pencil beam from B21, we found that a high tilt angle of the outer ring produces

the flat-topped soft pulse profile. This is expected because a flatter surface would mean a lesser change in the area of reprocessing, seen in figure 8. We also attempted one narrow Gaussian beam with a wider one, which reasonably gave the hard pulse profile with one narrow peak and one wide peak. We found that the other parameters are consistent with the previous B21 results. The model is simplistic and therefore was not able to reproduce the tertiary pulse profile peaks. We could attempt more complex models for the future work.

7. CONCLUSION

In our summer project, we performed spectral and timing analysis of Her X-1 during its main on superorbital phase. We used fifteen sets of NICER data that spans the end of the main-on and the beginning of the superorbital low state. We focused on the first four good data sets where the count rate is high enough to general detailed pulse profiles, while we are planing on further analyzing the data from a new set of observations in the future. The spectra of the first four good observations showed consistent shape, which only changes as the source enters into its superorbital low state. Our energy resolved pulse profiles show distinct behaviors in different energy ranges. The softest energy ranges show less variation than the hard energy ranges, which we propose to be caused by the obscuration of the accretion disk at the end of the main-on phase. We find some interesting initial constraints to the physical parameters of the accretion disk by disk modeling, although we leave more conclusive results to future work.
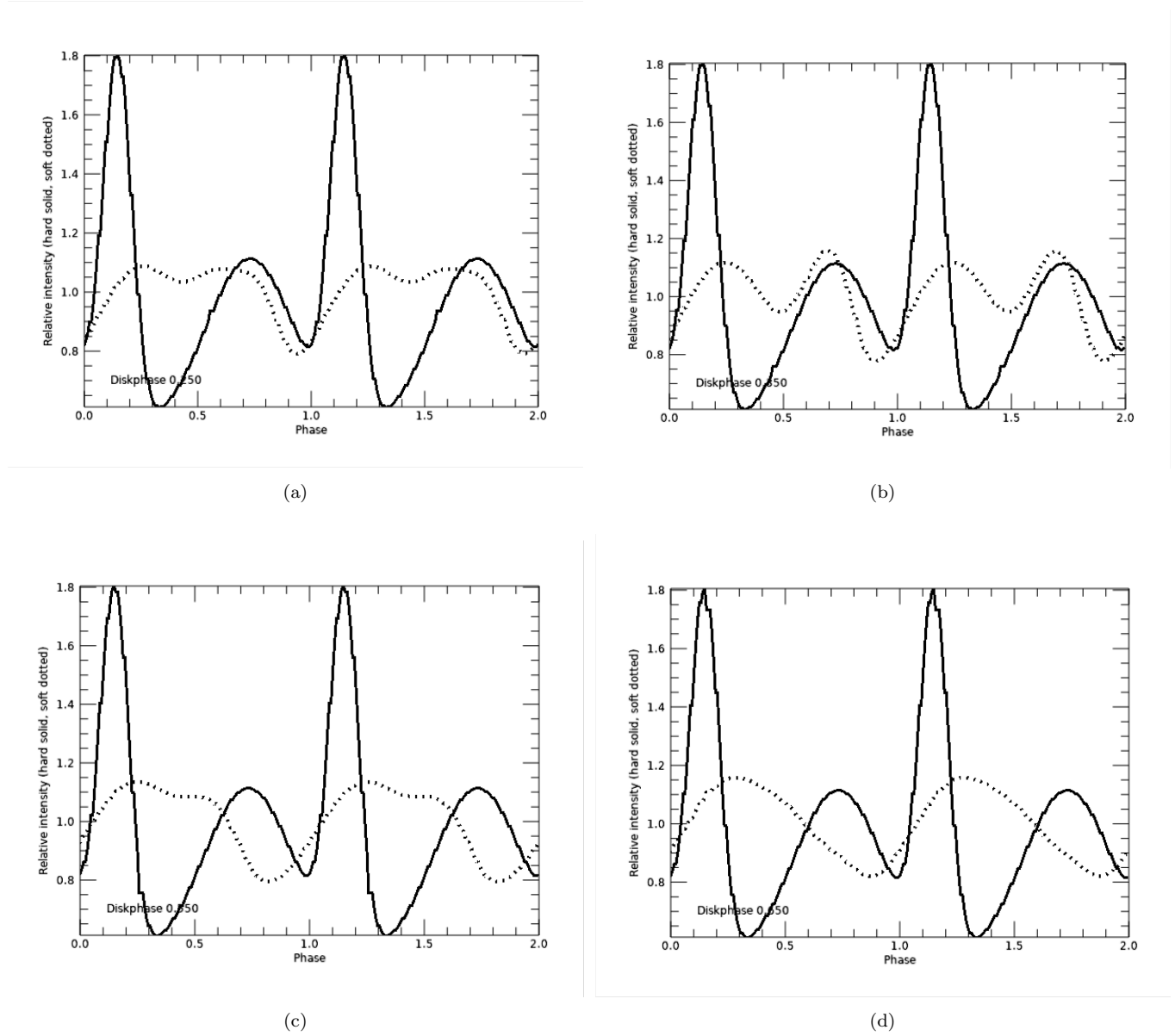
8. ACKNOWLEDGMENT

(a)

(b)

(c)

(d)

Figure 7. Simulated pulse profiles for superorbital phase (a) 0.250, (b) 0.350, (c) 0.550 and (d) 0.650. Our model was able to reproduce two noticeable secondary peaks at 0.250 superorbital phase similarly shaped to the NICER data. Our model was able to reproduce two noticeable secondary peaks at 0.350 superorbital phase similarly shaped to the NICER data. Similar to the the smaller peaks in (a), the soft and hard pulse profiles are better aligned. Around phase 0.250, we were able to align soft and hard pulse profile better than other phases so that more of the main soft peak is aligned with the secondary hard peaks. We were also able to reproduce the "flat" main soft peak at 0.550 superorbital phase. It can noticeably reproduce the secondary peak on the left edge of the flat top, which is seen in observation 06. We could also reproduce the round main soft peak at 0.650 superorbital phase similarly shaped to the B21 data. However, at these phases, we were not able to correctly align the phase of the soft and hard pulse profile so that the secondary hard peak is aligned with the main soft peak.
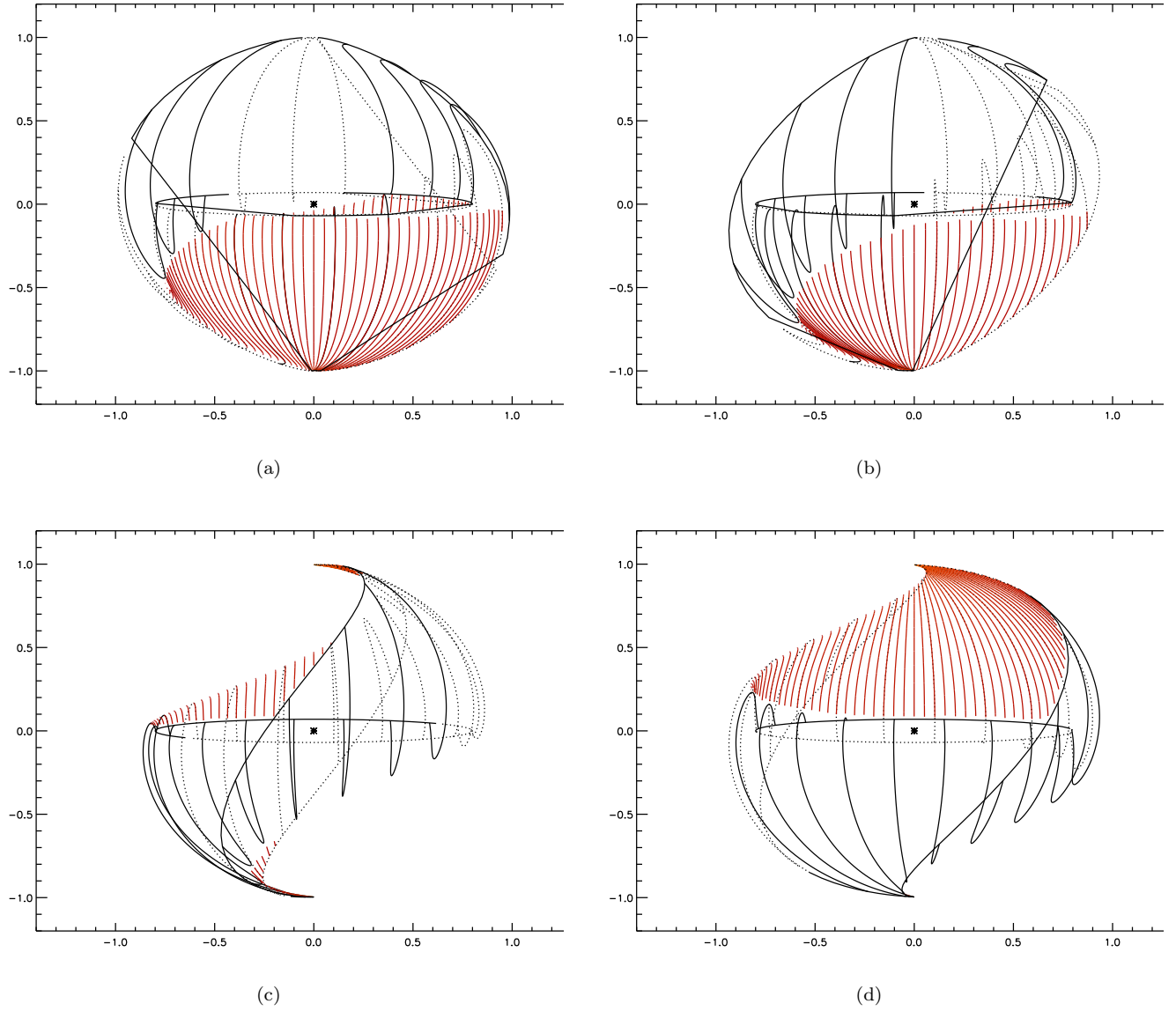
Figure 8. Simulated disk geometries with superorbital phase (a) 0.250, (b) 0.350, (c) 0.550 and (d) 0.650. The order here is the same as that in figure 7. The illuminated side of the side is shaded in orange and the back of the disk is shaded in white.

REFERENCES

Brumback, M. C., Hickox, R. C., Fürst, F. S., et al. 2020, ApJ, 888, 125, doi: 10.3847/1538-4357/ab5b04

—. 2021, ApJ, 909, 186, doi: 10.3847/1538-4357/abe122

Harrison, F. A., Craig, W. W., Christensen, F. E., et al. 2013, ApJ, 770, 103, doi: 10.1088/0004-637X/770/2/103

Hickox, R. C., & Vrtilek, S. D. 2005, The Astrophysical Journal, 633, 1064, doi: 10.1086/491596

Jimenez-Garate, M., Hailey, C., Herder, J., Zane, S., & Ramsay, G. 2002

Jones, C., & Forman, W. 1976, ApJL, 209, L131, doi: 10.1086/182283

Remillard, R. A., Loewenstein, M., Steiner, J. F., et al. 2021, An Empirical Background Model for the NICER X-ray Timing Instrument. https://arxiv.org/abs/2105.09901

Romanova, M. M., Ustyugova, G. V., Koldoba, A. V., & Lovelace, R. V. E. 2004, ApJ, 610, 920, doi: 10.1086/421867

Shakura, N., Prokhorov, M., Postnov, K., & Ketsaris, N. 1999, Astronomy and Astrophysics, 348

Truemper, J., Pietsch, W., Reppin, C., et al. 1978, ApJL, 219, L105, doi: 10.1086/182617